Three-Dimensional Osseointegration Patterns of Cementless Femoral Stems

An ex Vivo Study with High-Resolution Imaging and Histological Evaluation

Gilbert M. Schwarz, MD, Alexander Synek, PhD, Sascha Senck, PhD, Sam A. Kandathil, MD, Martin Holzleitner, MSc, Klemens Trieb, MD, Stephanie Huber, MD, Dieter Pahr, PhD, Jochen G. Hofstaetter, MD, and Lena Hirtler, MA, MD, PhD

Background: Osseointegration is essential for the long-term survival of cementless femoral stems and is dependent on periprosthetic bone quality and correct implantation technique. The aim of this study was to evaluate the 3-dimensional long-term fixation patterns of, and bone microarchitecture around, cementless hip stems.

Methods: Four specimens with varying degrees of bone quality and fixation characteristics from body donors who had received Alloclassic Zweymüller hip stems during their lifetime (mean time in situ at the time of death: 12.73 years) were evaluated with use of radiographs, high-resolution computed tomography (CT) scans, and hard-tissue histology. The CT voxel size was 85 μm, and the following parameters were calculated: total bone volume, total bone volume fraction, trabecular bone volume, trabecular bone volume fraction, cortical bone volume, cortical bone volume fraction, and cortical thickness. Bone-implant contact and canal fill index values for each Gruen zone of the specimens were calculated with use of histological samples.

Results: Femoral stems with apparently good cortical contact on clinical radiographs showed higher values for cortical bone volume, trabecular bone volume, and cortical thickness in the high-resolution CT analysis than femoral stems with apparently weak cortical contact on clinical radiographs. Based on the histological evaluation, the mean bone-implant contact ranged from 22.94% to 57.24% and the mean canal fill index ranged from 52.33% to 69.67% among the specimens.

Conclusions: This study demonstrated different osseointegration patterns of cementless femoral stems on the basis of radiographs, high-resolution CT scans, and histological evaluation. Femora with high cortical bone volume and cortical thickness were associated with higher canal fill indices, whereas femora with low cortical bone volume and cortical thickness had lower canal fill indices and showed a characteristic corner-anchorage pattern.

Clinical Relevance: Osseointegration patterns and thus the long-term survival of cementless femoral stems are dependent on cortical bone volume and cortical thickness.

The long-term outcome of cementless femoral stems is indicated by the amount of implant-bone fixation, which is dependent on a combination of primary mechanical and secondary biological fixation. Primary stability is achieved by press-fitting the prosthesis in the femur, and correct initial stability acts as the predominant influence on bone ongrowth[1]. Varying degrees of early micromotion from 20 to >150 μm lead to either predominantly bone or predominantly fibrous tissue formation[2]. Since undersizing of the femoral stem has been found to lead to early aseptic loosening or migration, parameters such as bone-implant contact and the canal fill index were established to calculate the correct stem size[3,4]. Stable osseointegration usually takes approximately 4 to 12 weeks and is the main factor responsible for the long-term survival of cementless implants[5].

Another important factor responsible for correct osseointegration is femoral bone quality and the underlying bone microarchitecture. Over the course of a human lifetime, constant bone remodeling leads to microarchitectural changes that result in increased fracture risks for elderly men and women[6,7]. Decreases in metaphyseal and diaphyseal bone mineral density following total hip arthroplasty have been found in the first year[8] as well as up to 6 years postoperatively[9]. Although increased fracture risk has been associated with low bone mineral density[10], no study thus far, to our knowledge, has demonstrated the bone microarchitecture around secondarily fixated femoral stems. Recent advances in microcomputed tomography (μCT) imaging have evidenced osseointegration of dental implants and small titanium femoral implants in animal

Disclosure: Part of this work was supported by the project entitled "TIMed 2022++ - Technological Innovation in Medicine 2022++", which is funded by the Regional Government of Upper Austria. The **Disclosure of Potential Conflicts of Interest** forms are provided with the online version of the article (http://links.lww.com/JBJS/H947).

models[11,12]. However, because of a lack of available human specimens and adequately large μCT scanners, no study to date has demonstrated correlations between standard radiographs and bone microarchitecture around femoral stems[13]. The resolution of clinical computed tomography (CT) scanners is not suitable for the evaluation of bone microarchitecture, and femoral hip stems that were implanted during a person's lifetime and retrieved post mortem are rare. Nonetheless, the prediction and improvement of fracture rates are important given the high morbidity and mortality associated with periprosthetic fractures[14], and a correct understanding of the underlying osseointegration patterns might help in this regard.

There are many different designs of femoral stems for total hip arthroplasty. One of the most frequently implanted cementless stems worldwide is the Alloclassic Zweymüller stem (Zimmer Biomet), which was invented in 1979. It is a tapered, conical stem with a grit-blasted surface and a rectangular cross section that obtains fixation primarily in the metaphysis and the proximal part of the diaphysis[15]. Long-term survival has been excellent, with rates of >96% over a time span of 20 to 30 years[16,17].

To add knowledge to the existing body of literature, we aimed to evaluate the 3-dimensional fixation patterns of cementless, tapered hip stems with a rectangular cross section. Four specimens with varying degrees of bone quality and fixation characteristics from body donors who had received Alloclassic Zweymüller hip stems during their lifetime were evaluated. The purpose was to demonstrate the underlying microarchitectural characteristics of osseointegration by making high-resolution CT scans and performing hard-tissue histological evaluation. We hypothesized that there are different secondary fixation patterns and that the pattern of fixation depends on anatomical conditions and implantation. By evaluating ex vivo implants in a prospective study setting, we intended to demonstrate different 3-dimensional secondary fixation patterns for the first time.

Materials and Methods

Our ex vivo study design involved 4 femora from different individuals, all of whom were female, with a mean time in situ at the time of death of 12.73 years. All femora had Alloclassic Zweymüller hip stems that had been implanted during the person's lifetime (Fig. 1). All specimens originated from the Vienna Medical Bio-/Implantbank of the Center for Anatomy and Cell Biology of the Medical University of Vienna, which was designed to prospectively collect all available specimens with hip implants from body donations to our institution. All donors provided informed written consent prior to their death to have their body utilized in medical education and research. The study was approved by the human ethics committee and the institutional review board of the Medical University of Vienna. Of the available specimens, we included those with varying degrees of cortical integration and bone

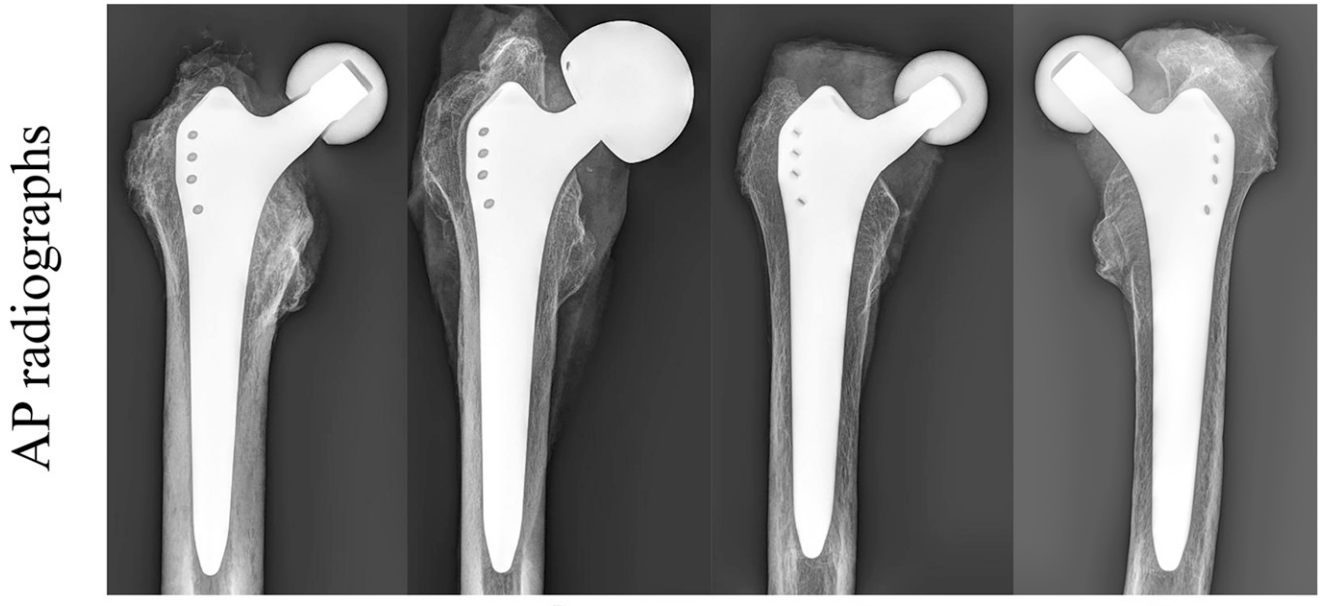

Specimen	A	B	C	D
Implant survival	8.1 years	8.1 years	12.4 years	>28 years*
Stem size	8	5	3	6
Patient age	82 years	80 years	88 years	103 years
Cortical integration	excellent	good	weak	weak
Characteristics	good bone quality	good bone quality, proximal lysis	poor bone quality	poor bone quality

Fig. 1

Overview of the included femoral specimens. AP = anteroposterior. *As a result of a policy limiting the retention of data to 30 years, the exact date of surgery for specimen D could not be specified.

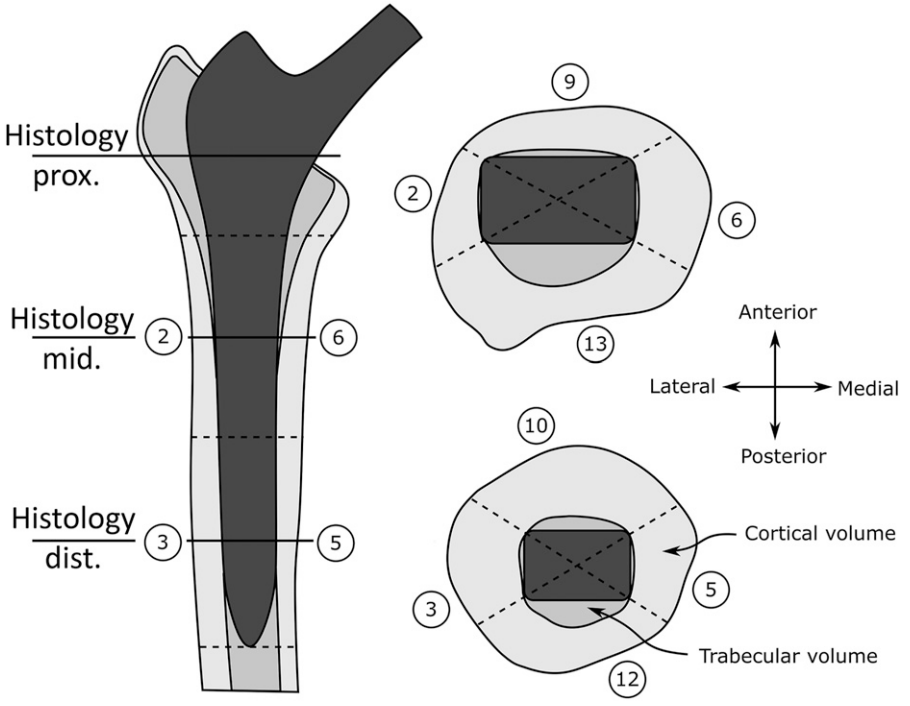

Fig. 2

Schematic illustration of the Gruen zones (numbered) that were utilized for high-resolution imaging and histological evaluation in this study.

quality based on a visual inspection of anteroposterior and lateral radiographs made in a standardized setting (Fig. 1).

Because of the long course of secondary biologic integration, none of the included specimens had an implant age of <1 year. Each femur was extracted from the body and stored at −20°C. Radiographs were assessed by the first author with guidance from the senior author and 1 senior EndoCert-classified surgeon. Specimen A had excellent cortical integration and good bone quality. Specimen B had good cortical integration, good bone quality, and lysis at the proximal part of the femur, around the implant stem. Specimens C and D had weak cortical integration and poor bone quality. All femora showed signs of osteopenia at the proximal part of the femur (Gruen zones 1 and 7). Immediate postoperative radiographs for specimens A and B and 1 radiograph from a routine follow-up examination 9 years postoperatively for specimen C were available (see Appendix Figure 1).

High-resolution CT image data acquisition at an isometric voxel size of 85 μm was performed with use of a RayScan 250 E cone-beam CT device using a PerkinElmer flat-panel detector with 2,048 × 2,048 pixels (pixel size, 200 μm) and a Viscom 225 kV microfocus x-ray tube. Optimal high-resolution CT scanning and reconstruction parameters were evaluated in an empirical parameter study. Because of the heights of the specimens, 2 consecutive scans were made for each specimen in order to image the whole femoral implant. Final CT scans were made at an x-ray tube voltage of 200 kV and a tube current of 300 μA. The integration time (i.e., the duration of the acquisition of a single x-ray projection) was 1,999 milliseconds. Each scan consisted of 1,440 projection images. To reduce beam-hardening artifacts, we utilized a physical 1-mm tin prefilter, as previously proposed by Schwarz et al.[18]. Subsequently, the 2 acquired image datasets obtained per sample were reconstructed and simultaneously aligned with use of X-AID (MITOS). X-AID features dedicated algorithms for image artifact reduction, including cupping and streaking artifact reduction. The correction of streaking artifacts is based on a normalized metal artifact reduction algorithm, which facilitates the reduction of streaking artifacts between and around highly attenuating metal parts[19]. The extent of artifact correction was determined empirically and checked qualitatively in order to reduce artifacts without introducing overcorrection[20]. Reconstruction parameters were empirically optimized for optimal image quality of the implant part with the greatest x-ray penetration length (i.e., the anterior part)[21]. Postprocessing and manipulation of the data were performed in VGSTUDIO MAX (version 3.5; Volume Graphics).

Quantitative CT Evaluation

A quantitative evaluation of high-resolution CT scans was performed with use of a morphometric analysis of the bone along the femoral stem. The middle and distal parts of the prosthesis were classified according to the Gruen zones (Fig. 2)[22]. The proximal region was not analyzed quantitatively as a result of larger image artifacts. The bone microstructure was segmented, and the total volume surrounding the implant was determined and was subdivided into cortical volume and trabecular volume (i.e., total volume minus cortical volume, and thus including both trabecular bone and marrow volume) according to a previously presented method[23]. The implant volume was excluded from all evaluations of bone volume. A region of 0.85 mm (10 voxels)

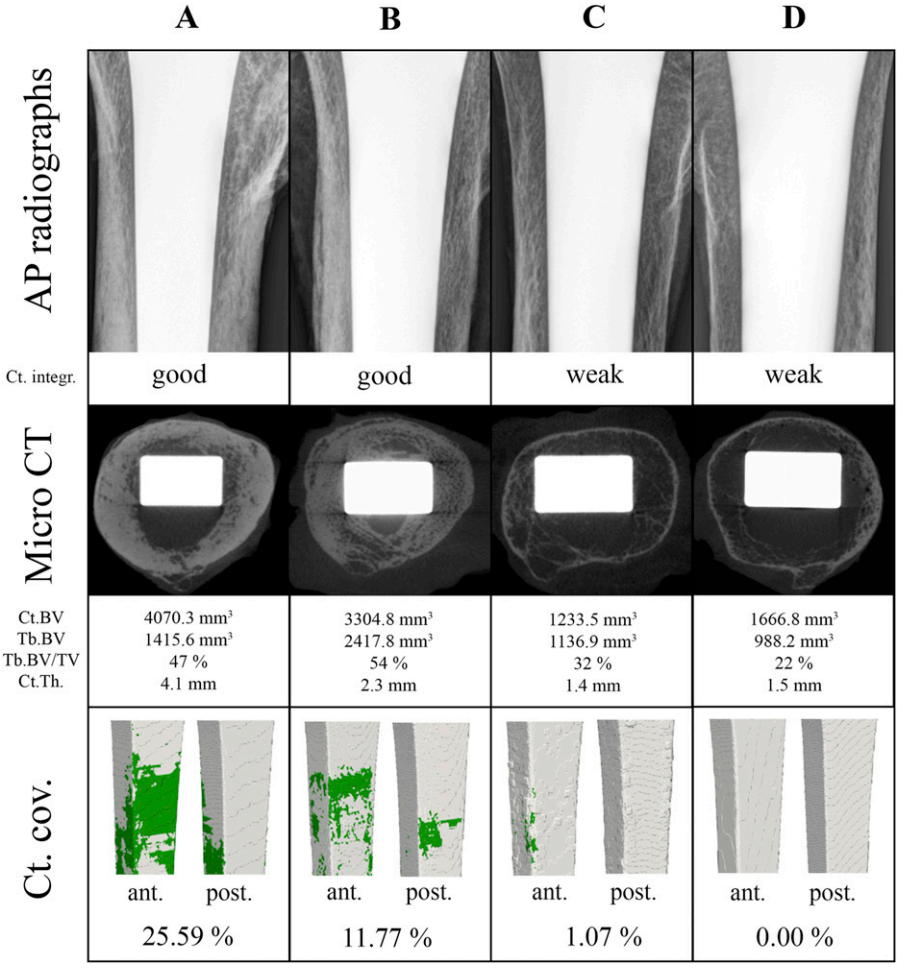

Fig. 3

Comparison of standard anteroposterior (AP) radiographs and high-resolution CT images of the middle region (i.e., Gruen zones 2, 6, 9, and 13) for each specimen. Ct. integr. = cortical integration, Ct.BV = cortical bone volume, Tb.BV = trabecular bone volume, Tb.BV/TV = trabecular bone volume fraction, Ct.Th. = cortical thickness, Ct. cov. = cortical coverage, ant. = anterior, post. = posterior.

around the implant was excluded from the analysis in order to reduce the influence of image artifacts. The following quantitative measures were evaluated for each Gruen zone: total bone volume, total bone volume fraction, trabecular bone volume, trabecular bone volume fraction, cortical bone volume, cortical bone volume fraction, and cortical thickness. In addition, the percentage of the implant surface in contact with the cortex was computed. This was achieved by dilating the implant volume by 1 voxel, counting the number of voxels that thereby became part of the cortical volume, and dividing that number of voxels by the total number of voxels of the implant surface. All image processing steps were performed in medtool (version 4.5; Dr. Pahr Ingenieurs e.U.).

Qualitative CT Evaluation

As a result of increased metal artifacts at the thicker proximal third of the stem, only a qualitative evaluation of this region was performed. Again, the stem was classified according to the Gruen zones (Fig. 2)[22]. The bone around the femoral stem was manually evaluated for lysis of >1 mm and osteopenia.

Histological Evaluation

Slices of 1 cm each were extracted from the middle of the proximal, middle, and distal thirds of each specimen (Fig. 2) with use of a diamond band saw (EXAKT 312 Pathology Saw; EXAKT Technologies). Following extraction, the specimens were fixed in Schaffer solution. They were then embedded in methylmethacrylate after the appropriate ascending series of alcohol solutions. Slices were ground, polished, and stained according to the Giemsa method. Each slice was evaluated for bone-implant contact with use of DotDotGoose software (American Museum of Natural History)[24], and bone-implant contact was reported as a percentage of the implant surface. Canal fill indices for the middle and distal regions were calculated with use of ImageJ (National Institutes of Health) to assess the stem size in relation to the femoral canal[4].

Statistical Analysis

Statistical analyses were performed with use of IBM SPSS Statistics for Windows (version 25.0) and a Microsoft Excel 365

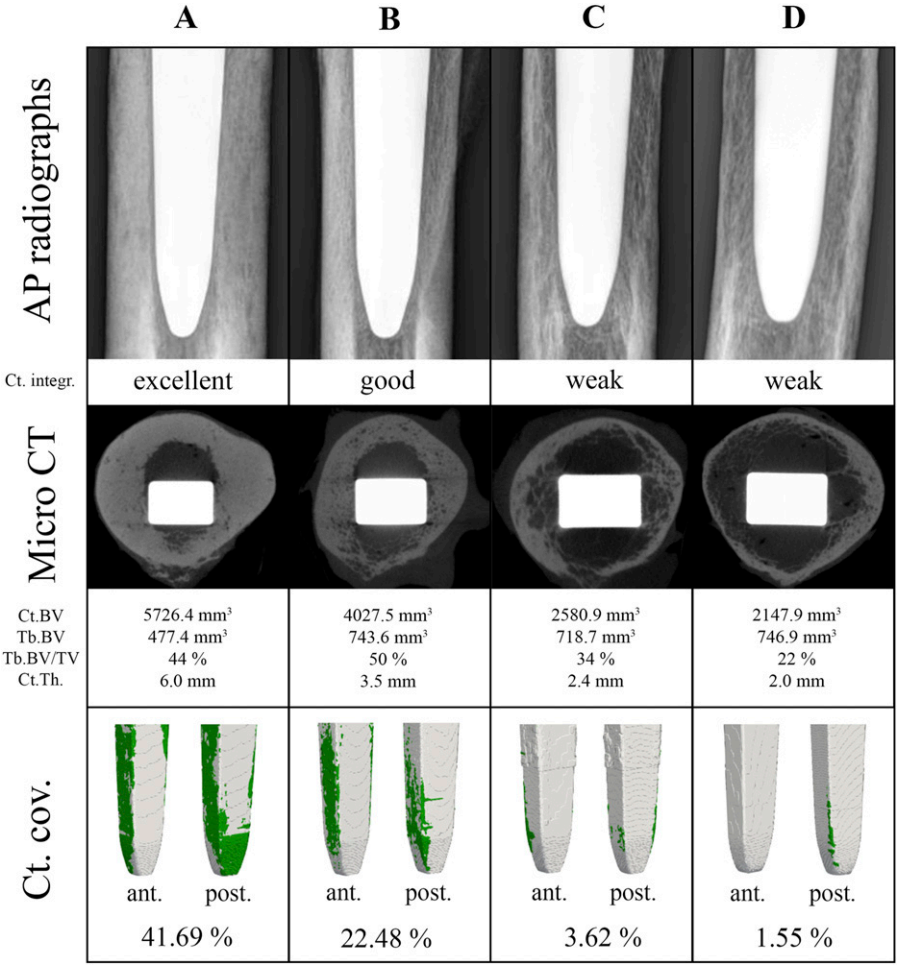

Fig. 4

Comparison of standard anteroposterior (AP) radiographs and high-resolution CT images of the distal region (i.e., Gruen zones 3, 5, 10, and 12) for each specimen. Ct. integr. = cortical integration, Ct.BV = cortical bone volume, Tb.BV = trabecular bone volume, Tb.BV/TV = trabecular bone volume fraction, Ct.Th. = cortical thickness, Ct. cov. = cortical coverage, ant. = anterior, post. = posterior.

spreadsheet. Descriptive statistics (mean, standard deviation, minimum, and maximum) were computed for all continuous variables. Bone-implant contact was measured with use of the point data collection method, and the following formula was utilized to report percentages: $\frac{Bone_{points}}{Bone_{points}+Void_{points}}\times 100$. The canal fill index was calculated with use of the following formula:

$$\left(\frac{implant_{width}}{canal_{width}}+\frac{implant_{length}}{canal_{length}}\right)\Big/2.$$

Results

Quantitative CT Evaluation

Specimens that demonstrated apparently good cortical contact on anteroposterior and lateral radiographs showed a tendency to have higher values for cortical bone volume, trabecular bone volume, trabecular bone volume fraction, and cortical thickness in the high-resolution CT analysis than specimens that demonstrated weak cortical contact on the radiographs. Comparisons of high-resolution CT scans and radiographs are presented in Figure 3 for the middle region and in Figure 4 for the distal region. All investigated specimens showed increasing values of cortical bone volume, cortical thickness, and cortical contact and decreasing values of trabecular bone volume from proximal to distal. The cortical contact areas at the middle and distal regions of the prosthesis were 32.64% for specimen A, 16.44% for specimen B, 2.17% for specimen C, and 0.69% for specimen D (Fig. 5). Detailed results of our high-resolution CT analysis can be found in Appendix Tables 1 through 4.

Qualitative CT Evaluation

Because of increased metal artifacts at the proximal region, only subjective, qualitative evaluations of high-resolution CT scans were performed for this region. All specimens showed signs of osteopenia, which was represented as visible thinning of trabecular bone at the proximal part of the prosthesis (Fig. 6). In addition, specimen B showed a distinct femoral bone lysis of >1 mm around the prosthesis.

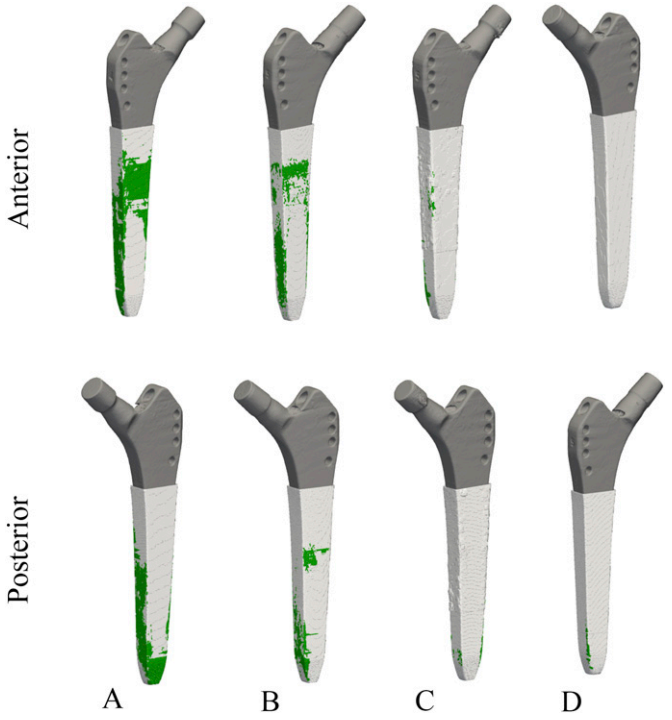

Fig. 5

Cortical contact areas of the whole stem of each specimen. Specimen A: 32.64%, B: 16.44%, C: 2.17%, and D: 0.69%.

Histological Evaluation

Good cortical integration was observed in the middle and distal slices for specimens A and B. In contrast, the proximal, middle, and distal slices for specimens C and D primarily demonstrated trabecular bone contact, with most of the bone contact at the edges of the prosthesis (Fig. 7). Bone-implant contact and canal fill index values for each Gruen zone of the specimens are presented in Table I. As in the qualitative CT analysis, the histological evaluation demonstrated visible thinning of the cancellous bone at the proximal part.

Discussion

The present study investigated 3-dimensional osseointegration patterns of secondarily fixated cementless hip stems by evaluating radiographs, high-resolution CT scans, and histology for well-osseointegrated hip stems and, to our knowledge, represents the first study of its kind in the literature. The most important finding of our study was the demonstration of different fixation patterns, characterized by different values for cortical bone volume, cortical thickness, bone-implant contact, and canal fill index.

The survival of cementless femoral stems depends on biological fixation between the bone and implant. Appropriate osseointegration, defined as bone ongrowth and a resulting implant-bone interface that is sufficient and stable, is crucial for the long-term survival of the implant[1]. Multiple studies

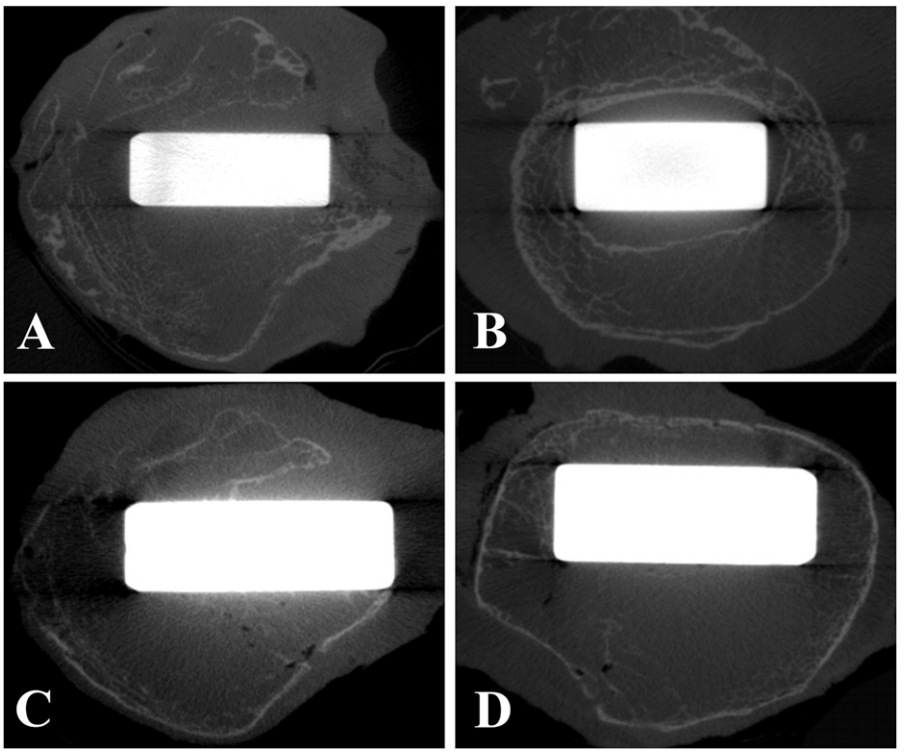

Fig. 6

High-resolution CT images of the proximal region for specimens A through D. The images demonstrate signs of osteopenia, represented as visible bone loss. Additionally, the image for specimen B shows distinct proximal lysis.

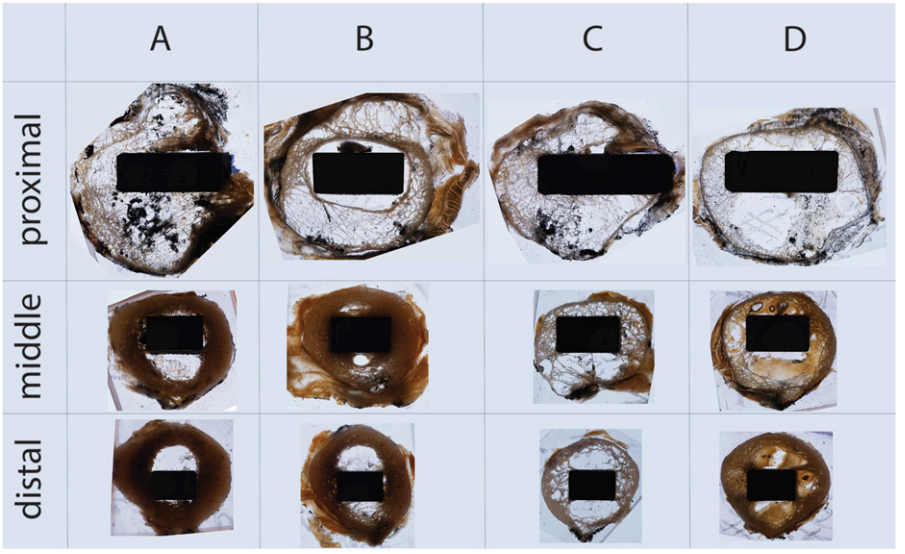

Fig. 7

Histological evaluation of the proximal, middle, and distal regions (Giemsa staining, ×1). "Proximal" represents Gruen zones 1, 7, 8, and 14; "middle," Gruen zones 2, 6, 9, and 13; and "distal," Gruen zones 3, 5, 10, and 12. Distinct lysis at the proximal section was observed for specimen B.

have focused on the fixation methods of hip implants, differentiating the types of ongrowth, degrees of stress-shielding, and initial postoperative cortical contact patterns and describing proximal bone density loss[9,25-27]. Although all of these studies included a relatively large number of patients, CT scans were only obtained after total hip arthroplasty, resulting in low image quality due to dose restrictions. To add knowledge to the existing body of literature, we aimed to evaluate different long-term osseointegration patterns of long, tapered femoral stems by utilizing a realistic ex vivo setting. Each hip stem had been implanted during the lifetime of the person and therefore represented the actual periprosthetic interface at a mean follow-up period of 12.73 years. We identified different fixation patterns in this sample, with specimens having either predominantly cortical or predominantly cancellous fixation. Specimens with high values for cortical bone volume and cortical thickness had higher values for cortical bone contact in the CT evaluation than those with low values for cortical bone volume and cortical thickness. The former were further characterized by slightly higher bone-implant contact and canal fill index values in the histological analysis. In contrast, specimens with low values for cortical bone volume and cortical thickness were associated with lower bone-implant contact and canal fill index values. The canal fill index was introduced as an indicator for the correct stem size, as an undersized stem with a canal fill index of <80% was shown to be associated with early aseptic loosening and stem migration[3]. In the present study, the specimens had a mean canal fill index of 62.3% and no signs of relevant aseptic loosening or stem migration. Although slightly different measurement heights (2 cm below the lesser trochanter versus the middle and distal Gruen zones) were utilized, our results suggest that even lower canal fill index values enable successful osseointegration.

In cases of small cortical thickness with no direct cortical contact, fixation is primarily achieved through cancellous bone contact at the corners of the prosthesis. The histological images in Figure 7 demonstrate different fixation patterns based on cortical thickness and cortical bone volume. The characteristic corner-anchorage pattern of primarily cancellous-fixated stems

TABLE I Bone-Implant Contact and Canal Fill Index on Histological Evaluation*

	Bone-Implant Contact (%)				Canal Fill Index (%)			
	A	B	C	D	A	B	C	D
Proximal	39.83	Lysis = 0.0	28.4	16.33	—	—	—	—
Middle	38.97	78.34	63.94	18.0	64.79	77.61	55.76	53.98
Distal	58.79	36.14	40.96	34.48	70.3	61.73	63.52	50.69
Mean	45.87	57.24†	44.43	22.94	67.54	69.67	59.64	52.33

*Proximal = Gruen zones 1, 7, 8, and 14; middle = Gruen zones 2, 6, 9, and 13; distal = Gruen zones 3, 5, 10, and 12. †The mean was based only on the middle and distal slices because of the lysis at the proximal region.

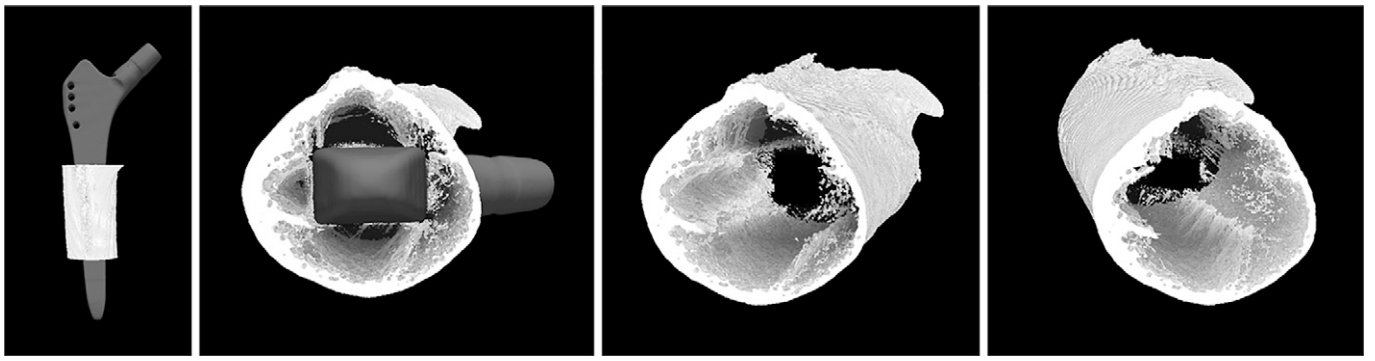

Fig. 8

Three-dimensional renderings of a typical cancellous bone corner-anchorage pattern, generated from images of the middle region in specimen D. This pattern was observed in both specimens C and D.

such as those in specimens C and D is further supported by the 3-dimensional CT renderings presented in Figure 8. Coathup et al.[28] evaluated postmortem-retrieved hip implants and compared bone ongrowth for different surface coatings histologically. They found more bone ongrowth at the medial plane than at the lateral plane and reported a tendency for overall bone ongrowth to increase with longer implant duration. However, it is difficult to compare their findings with our own because different stems (rectangular versus round), different surface coatings, and different heights (measured at a Gruen zone versus measured at the metaphysis) were investigated.

Signs of osteopenia with thinning of the trabecular bone at the proximal part of the femur were found in all investigated specimens in both the high-resolution CT analysis (Fig. 6) and the histological analysis (Fig. 7). Given the diaphyseal anchorage mechanism of Alloclassic Zweymüller stems, this finding can be interpreted as evidence of stress-shielding and is in line with previous reports[25,27]. Engh et al.[25] differentiated among 4 different stages of stress-shielding on the basis of radiographic findings. In the present study, stress-shielding was analyzed with use of high-resolution CT scans and histology, and thus the initial radiographic classification system of Engh et al.[25] could not be utilized in this scenario.

The primary limitation of the present study is the low number of specimens that were included, and therefore general conclusions cannot be drawn as it is possible that other osteointegration patterns exist that were not observable in our cohort. Likewise, since the Alloclassic Zweymüller stem has a grit-blasted titanium surface without hydroxyapatite coating and the present study was dependent on voluntary body donors who received hip stems during their lifetime, no comparisons can be drawn to stems with hydroxyapatite coating. However, by focusing on the Alloclassic Zweymüller stem, which is one of the most frequently implanted hip systems in the world[17], we present a unique in-depth look into fixation mechanisms and the underlying microarchitecture. Another limitation is the fact that the bone microarchitecture around the proximal part of the prosthesis could not be quantified with CT; however, it was included in the histological analysis. Although we utilized an optimized scanning and reconstruction routine for femoral implants via artifact reduction software dedicated to industrial high-resolution CT, it was not possible to completely eliminate all artifacts from CT scanning in the final volume datasets, as described by Trieb et al.[21]. These remaining artifacts and the comparatively low resolution for the bone morphometric analysis must also be kept in mind when interpreting the quantitative results of this study. Another limitation might be the method of automating the measurement of cortical and trabecular bone volume based on a certain threshold, as previously reported[23]. Nonetheless, the CT image quality and histological evaluation in the present study are still superior to those in previous studies in which clinical CT scans for longitudinal bone mineral density evaluation were utilized or stems were implanted in anatomical samples post mortem. A major limitation of the previous studies involving postmortem implantation is the inability to simulate osseointegration and the changes to bone over years. To our knowledge, the present study is the first comprehensive assessment of the fixation patterns of secondarily fixated cementless femoral stems based on a combination of high-resolution CT scans and histology.

Conclusions

This study demonstrated different osseointegration patterns of cementless femoral stems on the basis of radiographs, high-resolution CT scans, and histological evaluation. Femora with high cortical bone volume and cortical thickness were associated with higher canal fill indices, whereas femora with low cortical bone volume and cortical thickness had lower canal fill indices and showed a characteristic corner-anchorage pattern.

Appendix

eA Supporting material provided by the authors is posted with the online version of this article as a data supplement at jbjs.org (http://links.lww.com/JBJS/H948). ■

NOTE: The authors thank the body donors and their families, as such studies would not be possible without their donation and support.

Gilbert M. Schwarz, MD[1,2,3]
Alexander Synek, PhD[4]
Sascha Senck, PhD[5]
Sam A. Kandathil, MD[2]

Martin Holzleitner, MSc[5]
Klemens Trieb, MD[6]
Stephanie Huber, MD[2,3]
Dieter Pahr, PhD[4,7]
Jochen G. Hofstaetter, MD[3,8]
Lena Hirtler, MA, MD, PhD[2]

[1]Department of Orthopedics and Trauma-Surgery, Medical University of Vienna, Vienna, Austria

[2]Center for Anatomy and Cell Biology, Medical University Vienna, Vienna, Austria

[3]Michael Ogon Laboratory for Orthopedic Research, Orthopedic Hospital Vienna, Vienna, Austria

[4]Institute for Lightweight Design and Structural Biomechanics, Technical University of Vienna, Austria

[5]Research Group Computed Tomography, University of Applied Sciences Upper Austria, Wels, Austria

[6]Department of Orthopaedic and Trauma Surgery, Paracelsus Medical University Salzburg, Salzburg, Austria

[7]Division Biomechanics, Karl Landsteiner University of Health Sciences, Krems an der Donau, Austria

[8]2nd Department, Orthopaedic Hospital Vienna Speising, Vienna, Austria

Email for corresponding author: lena.hirtler@meduniwien.ac.at

References

1. Chanda S, Mukherjee K, Gupta S, Pratihar DK. A comparative assessment of two designs of hip stem using rule-based simulation of combined osseointegration and remodelling. Proc Inst Mech Eng H. 2020 Jan;234(1):118-28.

2. Pilliar RM, Lee JM, Maniatopoulos C. Observations on the effect of movement on bone ingrowth into porous-surfaced implants. Clin Orthop Relat Res. 1986 Jul;(208):108-13.

3. Fottner A, Woiczinski M, Kistler M, Schröder C, Schmidutz TF, Jansson V, Schmidutz F. Influence of undersized cementless hip stems on primary stability and strain distribution. Arch Orthop Trauma Surg. 2017 Oct;137(10):1435-41.

4. Laine HJ, Pajamäki KJ, Moilanen T, Lehto MU. The femoral canal fill of two different cementless stem designs. The accuracy of radiographs compared to computed tomographic scanning. Int Orthop. 2001;25(4):209-13.

5. Zweymüller KA, Lintner FK, Semlitsch MF. Biologic fixation of a press-fit titanium hip joint endoprosthesis. Clin Orthop Relat Res. 1988 Oct;(235):195-206.

6. Farr JN, Khosla S. Determinants of bone strength and quality in diabetes mellitus in humans. Bone. 2016 Jan;82:28-34.

7. Samelson EJ, Broe KE, Xu H, Yang L, Boyd S, Biver E, Szulc P, Adachi J, Amin S, Atkinson E, Berger C, Burt L, Chapurlat R, Chevalley T, Ferrari S, Goltzman D, Hanley DA, Hannan MT, Khosla S, Liu CT, Lorentzon M, Mellstrom D, Merle B, Nethander M, Rizzoli R, Sornay-Rendu E, Van Rietbergen B, Sundh D, Wong AKO, Ohlsson C, Demissie S, Kiel DP, Bouxsein ML. Cortical and trabecular bone microarchitecture as an independent predictor of incident fracture risk in older women and men in the Bone Microarchitecture International Consortium (BoMIC): a prospective study. Lancet Diabetes Endocrinol. 2019 Jan;7(1):34-43.

8. Steens W, Boettner F, Bader R, Skripitz R, Schneeberger A. Bone mineral density after implantation of a femoral neck hip prosthesis—a prospective 5 year follow-up. BMC Musculoskelet Disord. 2015 Aug 12;16:192.

9. Mueller LA, Nowak TE, Haeberle L, Mueller LP, Kress A, Voelk M, Pfander D, Forst R, Schmidt R. Progressive femoral cortical and cancellous bone density loss after uncemented tapered-design stem fixation. Acta Orthop. 2010 Apr;81(2):171-7.

10. Greenspan SL, Myers ER, Maitland LA, Resnick NM, Hayes WC. Fall severity and bone mineral density as risk factors for hip fracture in ambulatory elderly. JAMA. 1994 Jan 12;271(2):128-33.

11. He T, Cao C, Xu Z, Li G, Cao H, Liu X, Zhang C, Dong Y. A comparison of micro-CT and histomorphometry for evaluation of osseointegration of PEO-coated titanium implants in a rat model. Sci Rep. 2017 Nov 24;7(1):16270.

12. López-Valverde N, López-Valverde A, Cortés MP, Rodríguez C, Macedo De Sousa B, Aragoneses JM. Bone Quantification Around Chitosan-Coated Titanium Dental Implants: A Preliminary Study by Micro-CT Analysis in Jaw of a Canine Model. Front Bioeng Biotechnol. 2022 Apr 7;10:858786.

13. Liu S, Broucek J, Virdi AS, Sumner DR. Limitations of using micro-computed tomography to predict bone-implant contact and mechanical fixation. J Microsc. 2012 Jan;245(1):34-42.

14. Bhattacharyya T, Chang D, Meigs JB, Estok DM 2nd, Malchau H. Mortality after periprosthetic fracture of the femur. J Bone Joint Surg Am. 2007 Dec;89(12):2658-62.

15. Zweymüller K, Semlitsch M. Concept and material properties of a cementless hip prosthesis system with Al2O3 ceramic ball heads and wrought Ti-6Al-4V stems. Arch Orthop Trauma Surg (1978). 1982;100(4):229-36.

16. Kolb A, Grübl A, Schneckener CD, Chiari C, Kaider A, Lass R, Windhager R. Cementless total hip arthroplasty with the rectangular titanium Zweymüller stem: a concise follow-up, at a minimum of twenty years, of previous reports. J Bone Joint Surg Am. 2012 Sep 19;94(18):1681-4.

17. Pisecky L, Hipmair G, Schauer B, Böhler N. 30-years of experience with the cementless implanted Alloclassic total hip arthroplasty system-An ultra-long-term follow-up. J Orthop. 2017 Nov 6;15(1):18-23.

18. Schwarz GM, Huber S, Wassipaul C, Kasparek M, Hirtler L, Hofstaetter JG, Bader T, Ringl H. Influence of Scan Parameters of Single and Dual-Energy CT Protocols in Combination with Metal Artifact Suppression Algorithms for THA: An ex Vivo Study. J Bone Joint Surg Am. 2023 Apr 19;105(8):620-9.

19. Meyer E, Raupach R, Lell M, Schmidt B, Kachelriess M. Normalized metal artifact reduction (NMAR) in computed tomography. Med Phys. 2010 Oct;37(10):5482-93.

20. Glinz J, Zabler S, Kastner J, Senck S. Metal Artifacts in Attenuation and Phase Contrast X-Ray Microcomputed Tomography: A Comparative Study. Experimental Mechanics. 2022;62(5):837-47.

21. Trieb K, Glinz J, Reiter M, Kastner J, Senck S. Non-Destructive Testing of Ceramic Knee Implants Using Micro-Computed Tomography. J Arthroplasty. 2019 Sep;34(9):2111-7.

22. Gruen TA, McNeice GM, Amstutz HC. "Modes of failure" of cemented stem-type femoral components: a radiographic analysis of loosening. Clin Orthop Relat Res. 1979 Jun;(141):17-27.

23. Pahr DH, Zysset PK. From high-resolution CT data to finite element models: development of an integrated modular framework. Comput Methods Biomech Biomed Engin. 2009 Feb;12(1):45-57.

24. American Museum of Natural History. DotDotGoose. Accessed 2024 Feb 6. https://biodiversityinformatics.amnh.org/open_source/dotdotgoose/.

25. Engh CA, Bobyn JD, Glassman AH. Porous-coated hip replacement. The factors governing bone ingrowth, stress shielding, and clinical results. J Bone Joint Surg Br. 1987 Jan;69(1):45-55.

26. Kobayashi K, Osaki M, Kidera K, Ait-Si-Selmi T, Ramos-Pascual S, Saffarini M, Bonnin MP. Stem-bone contact patterns of a long straight tapered uncemented stem for primary THA. Arch Orthop Trauma Surg. 2022 Dec;142(12):4063-73.

27. Wada H, Mishima H, Sugaya H, Nishino T, Yamazaki M. Three-Dimensional Analysis of the Contact Pattern between the Cortical Bone and Femoral Prosthesis after Cementless Total Hip Arthroplasty. Adv Orthop. 2016;2016:8052380.

28. Coathup MJ, Blunn GW, Flynn N, Williams C, Thomas NP. A comparison of bone remodelling around hydroxyapatite-coated, porous-coated and grit-blasted hip replacements retrieved at post-mortem. J Bone Joint Surg Br. 2001 Jan;83(1):118-23.